

Generating Multimodal Textures with a Soft Hydro-Pneumatic Haptic Ring

Ana Sanz Cozcolluela^a, Yasemin Vardar^{*a}

^a*Department of Cognitive Robotics, Delft University of Technology, Mekelweg 2, Delft, 2628 CD, The Netherlands*

Abstract

The growing adoption of extended reality (XR) has driven demand for wearable technologies that can replicate natural tactile sensations and allow users to interact freely with their surroundings using bare fingers. However, most existing wearable haptic technologies that support such free interactions can deliver sensations across limited tactile modalities. Here, we introduce a soft haptic ring and a data-driven rendering methodology to generate multimodal texture sensations. The device integrates pneumatic and hydraulic actuation to simulate roughness, thermal, and softness cues on the proximal phalanx, enabling users to explore surroundings naturally with their fingertips. The rendering methodology dynamically modulates those cues based on the user's exploratory actions. We validated our approach by conducting a user study with 15 participants, who matched six virtual textures generated by the ring to their real counterparts and rated their perceived sensations. Participants achieved up to 90% accuracy in texture matching. The adjective ratings confirmed that the ring delivers distinct, perceptually rich stimuli across all rendered sensations. These findings highlight the ring's potential for immersive XR applications, offering diverse tactile feedback without restricting physical interaction.

Keywords: Wearable, Haptics, Multimodal, Multisensory, Extended Reality, Texture Rendering,

1. Introduction

Our tactile experiences with our surroundings profoundly shape our understanding of the world. Through touch, we interpret physical properties and manipulate objects with precision. Yet, in digital environments, these rich tactile interactions are mainly absent. Wearable haptic devices, which gained special interest from academia and industry in the last decade, aim to bridge this gap by simulating naturalistic tactile cues through mechatronic components worn on the body.

However, most state-of-the-art wearable haptic devices adopt glove-like designs, which, despite their intuitive interfaces, are often cumbersome, heavy, and restrictive (Pacchierotti et al., 2017). These designs can hinder hand movements and, since they typically cover the fingertips, pose challenges for finger tracking and natural interaction with the environment (Pacchierotti et al., 2016). This issue is especially problematic in mixed and augmented reality applications, where users engage with physical environments enhanced by artificial sensations when desired (Teng and Lopes, 2022).

Wearable haptic devices that can stimulate other body parts, thereby freeing the fingertips, offer a potential solution for embedding artificial tactile sensations in physical environments when desired (Pacchierotti et al., 2016; van Riessen and Vardar, 2023; Sun et al., 2022; de Vlam et al., 2023). However, despite their growing popularity, these devices face challenges related to weight, flexibility, and ease of wear. Many rely on rigid and bulky materials that conflict with the flexible nature of the human body, limiting both comfort and the fidelity of tactile interactions (El Saddik, 2007).

Recently, soft haptic devices—designed as rings (Talhan et al., 2020; Han et al., 2018), wristbands (Zhang and Sra, 2021; Liu et al., 2021), or sleeves (Zhu et al., 2020; Goetz et al., 2020)—have been proposed to enhance wearability by conforming more naturally to the skin. Among these, pneumatic-based devices have gained popularity due to

*Corresponding author

their fast response times, cost-effectiveness, and high power-to-weight ratios. While pneumatic systems dominate, hydraulic actuation offers an alternative with improved drive efficiency and dynamic performance.

These soft wearable devices can also be designed to deliver a wide range of tactile sensations to enhance the naturalism and information richness of virtual interactions. For instance, the multimodal soft ring by Talhan et al. (2020) provided static pressure, high-frequency vibration, and impact force feedback through controlled pneumatic inflation. Similarly, the hydraulic ring demonstrated by Han et al. (2018) combined pressure and vibration cues with thermal stimulation by circulating water at different temperatures. Other studies, such as Zhang and Sra (2021); Liu et al. (2021); Goetz et al. (2020), integrated pressure and thermal actuation in soft wristbands or sleeves.

Despite their potential for displaying a wide variety of tactile sensations, most wearable haptic devices (whether soft or hard) primarily deliver basic sensations, such as discrete forces, temperatures, or vibrations, rather than rich textural experiences. Only a few studies explicitly focus on tactile texture rendering. For instance, the multimodal haptic thimbles by Talhan et al. (2022); Hashem et al. (2022) or vibrotactile rings by Gaudeni et al. (2019); Friesen and Vardar (2024); Normand et al. (2025) simulate roughness through vibration but overlook other sensations like softness and temperature, which were found to be critical perceptual dimensions for perception of natural surfaces (Okamoto et al., 2013). To achieve rendering textures with these perceptual dimensions, designed haptic devices should independently deliver vibration, pressure, and thermal cues.

In this study, we present a soft haptic ring and a data-driven rendering approach for displaying multimodal textures. The ring, made entirely from silicone, independently delivers vibrotactile, pressure, and thermal cues to the proximal phalanx while allowing full-hand motion and unrestricted exploration (see Figure 1). Our design combines a hydraulic circuit for thermal stimulation with a pneumatic chamber for pressure and vibrotactile feedback, both selectively controlled based on the user's exploratory actions.

We validated our design and rendering methodology through a user study in which 15 participants matched six virtual textures generated by the ring to their real counterparts and rated their perceived sensations. To the best of our knowledge, this is the first soft ring to integrate multiple actuation mechanisms and three haptic modalities within a single interface. Furthermore, no existing rendering methodology combines all these modalities in a data-driven approach. While an earlier work (Kodak and Vardar, 2023) demonstrated displaying these modalities through a pen device, they only focused solely on artificial textures rather than replicating real surfaces.

This paper is organized as follows. Section 2.1 describes the design of the device and the fabrication process. Section 2.2 explains the details of the device control. Section 2.3 elucidates the texture rendering methodology. Section 2.4 details the user study to validate the proposed device and rendering approach. The results of the user study are presented in Section 3 and further elaborated in Section 4. Finally, Section 5 summarizes the key findings and conclusions.

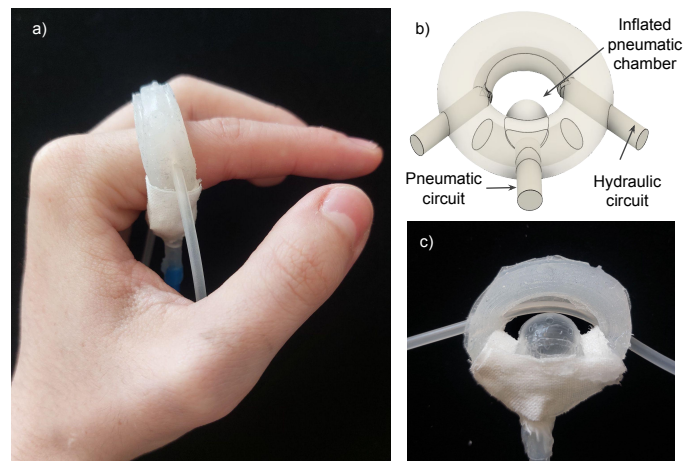


Figure 1: a) The soft haptic ring worn on the finger. b) The ring can provide multisensory cutaneous feedback via fluidic actuators. A pneumatic chamber at the finger's base provides pressure and vibration cues, while a coiled hydraulic tube around the proximal phalanx transmits thermal sensations. c) The pneumatic actuator is in inflated mode.

2. Materials and Methods

2.1. Device Design and Fabrication

We aimed to overcome the limitations of existing works by developing a new device with the following key requirements:

1. A flexible, lightweight, and compact form factor for ease of use.
2. A design that leaves the user's fingertip unobstructed, enabling natural interaction with the physical environment.
3. The ability to provide multimodal tactile stimuli, such as pressure, vibration, and thermal, relevant for texture perception.
4. The capability to deliver these tactile cues both independently and simultaneously.

We addressed the first and second requirements by opting for a soft ring fabricated entirely from silicone as our haptic interface. A ring design ensures the fingertip remains unobstructed, allowing for natural hand movements and unrestricted environment exploration. Similarly, by manufacturing the ring out of silicone, flexibility, lightweightness, and compactness are maximized while allowing for easy production of various sizes that accommodate different finger sizes.

The third requirement presents a challenge when working with a soft interface. Thermal stimuli are typically generated using thermoelectric devices (Jones and Ho, 2008), but their rigid nature could undermine the flexibility of our soft ring. Similarly, while piezoelectric actuators can produce complex vibration patterns (Biswas and Visell, 2019), their integration would compromise the soft character of the ring. Hence, we opted for a hybrid design combining hydraulic and pneumatic systems to address these challenges (see Figure 1b). The hydraulic system circulates water at varying temperatures through the ring to provide the desired thermal stimuli. Concurrently, the pneumatic system inflates a chamber within the ring to create vibratory cues through rapid inflation and deflation. Additionally, by modulating the inflation patterns of the chamber, the pneumatic system can provide pressure stimuli. This dual-actuation approach enables thermal and vibratory feedback and satisfies the fourth requirement, as both systems function independently and can simultaneously generate multimodal stimuli.

In our design, the pneumatic chamber is positioned on the underside of the ring, in contact with the ventral side of the finger's proximal phalanx (check Figure 1b and c). On the upper side of the ring, which makes contact with the dorsal phalanx, a thin silicone tube forming part of the hydraulic circuit is placed. Instead of designing an embedded hydraulic chamber like the pneumatic one, we inserted a silicone tube directly into a cavity designed on the ring to maximize thermal conductivity.

For the fabrication of our soft ring, we chose EcoFlex 00-30 as the primary material due to its favorable properties. Its elastic modulus ranges from 100 to 125 kPa and falls within the range of human skin (Kalra et al., 2016), ensuring a natural feel. This material's softness, strength, and stretchability make it an ideal choice for wearable and skin-attachable devices (Rameshwar et al., 2023).

The ring fabrication process involved multiple steps. First, we 3D-printed two identical plastic molds to form the two halves of the ring. These molds, made from polylactic acid (PLA), were designed to split the ring along its transversal plane and were further divided into two parts to facilitate demolding. We prepared three mold variations to accommodate different finger sizes with internal diameters of 15, 18.5, and 22 mm. We ensured that the pneumatic chamber maintained a constant volume across all ring sizes to exhibit similar inflation characteristics.

The next step in the fabrication process was casting the molds. This step begins with mixing the parts of EcoFlex silicone rubber (Part A and Part B). After thorough stirring, the molds were coated with a release agent to facilitate demolding, and the mixture was poured in and then left to cure for at least four hours at room temperature. Once cured, the two halves were bonded using the same silicone mix. At this stage, a 4 mm diameter silicone tube was inserted between the halves, allowing for future inflation of the pneumatic chamber. Precise alignment of all components was crucial to ensure a durable and well-functioning final product. We also reinforced the insertion area by lining Teflon tape, then coating it with a layer of DragonSkin 30 cured for seventeen hours. The higher Young's modulus of this silicone mix, combined with the thin Teflon tape layer, provided structural support by preventing leakage or bursting at high pressures. During this process, it was crucial to apply the new silicone mix only at the tube insertion while ensuring the inner part of the ring remained uncovered. This precaution preserved the actuator's inflation characteristics.

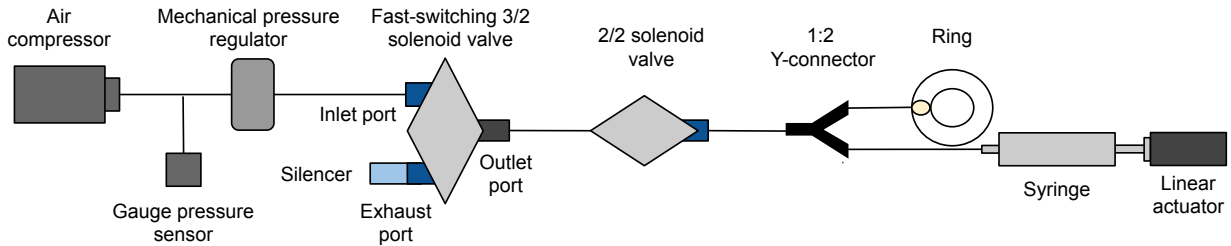


Figure 2: Schematic of the pneumatic circuit. The 2/2 solenoid valve remains open to generate vibration cues and is closed for pressure cues.

During the final step of the manufacturing process, a strain-limiting fabric layer was applied to the ring’s upper, lower, and outer surfaces using Sil-Poxy silicone adhesive. This process ensured that when air filled, only the ring’s inner surface would inflate and provide localized pressures at the frontal side of the phalanx. Additionally, during this step, a thin 2 mm silicone tube connected to the hydraulic circuit to present thermal cues was embedded on the inner surface of the ring.

2.2. Device Control

In our soft haptic ring, the pressure and vibration cues are generated through a pneumatic circuit connected to the ring’s pneumatic chamber, as seen in Figure 2. This circuit includes two different sections connected in parallel to generate pressure and vibration stimuli, respectively.

The primary component for generating vibration cues is a fast-switching three-way solenoid pneumatic valve (MHE2-MS1H-3/2G-M7, Festo), selected for its high 300 Hz switching frequency. The valve’s inlet port is supplied by an air compressor (FD-186, Fengda), with pressure regulated at 75 kPa using a mechanical pressure regulator (AR-200, LNCN) and monitored by a digital pressure gauge. This pressure level ensures perceivable inflation of the ring while preventing excessive force that could lead to bursting. The output port of the valve is connected to the ring via a 1:2 Y-connector, while the exhaust port is fitted with a silencer to reduce noise. This configuration allows air to flow freely into the ring when the active valve inflates the actuator. When inactive, the air is blocked at the inlet while the ring is connected to the exhaust, enabling rapid deflation. Consequently, the quick activation and deactivation of the solenoid valve produces vibratory cues through rapid inflation and deflation of the ring.

Although this valve could theoretically provide pressure cues by adjusting switching times, it proved challenging to control inflation rates precisely using this method. Additionally, this setup did not allow air to be retained inside the ring or expelled at variable speeds, limiting its ability to simulate materials of different stiffness or maintain inflation for prolonged contact sensations. Hence, a pressure rendering system was added in parallel to the vibration valve via the Y-connector to address these limitations. This pressure rendering system consists of a linear actuator controlling a syringe connected to the ring. The ring can exhibit various inflation profiles by adjusting the actuator’s speed. However, due to the low operating pressures of the circuit, the fast-switching solenoid valve exhibited minor leakage in its closed state, preventing the ring from maintaining inflation. Hence, an additional normally closed two-way solenoid valve (MHA1-M1H-2/2G-0.9-PI, Festo) was inserted between the vibration valve and the Y-connector. In this way, the valve remains open to provide vibratory stimuli, allowing air to flow to the ring. Conversely, when providing pressure stimuli, the valve closes, enabling the ring to inflate, maintain its inflation, or deflate based on the operation of the linear actuator controlling the syringe.

The thermal cues were delivered by regulating the water temperature inside the silicone tube via a hydraulic circuit, as illustrated in Figure 3. The circuit comprised a hot and cold tank, whose water was mixed in a central container before being pumped to the ring. The hot water tank maintained a constant temperature of 42.5 °C, regulated by a 300 W submersible heating element (860-6921, RS PRO). The cold water tank was kept below 5 °C by continuously adding ice. Water from these tanks was transferred to the mixing container using two independent pumps (KW-1646, Kiwi Electronics), from which a third pump directed the mixed water through the silicone tube embedded in the ring. After circulating, the water returned to the mixing tank, completing the cycle.

Although using a mixing tank rather than directly pumping hot or cold water to the ring introduced a slight delay in reaching target temperatures, it ensured more uniform mixing and better temperature stability. The water level in the

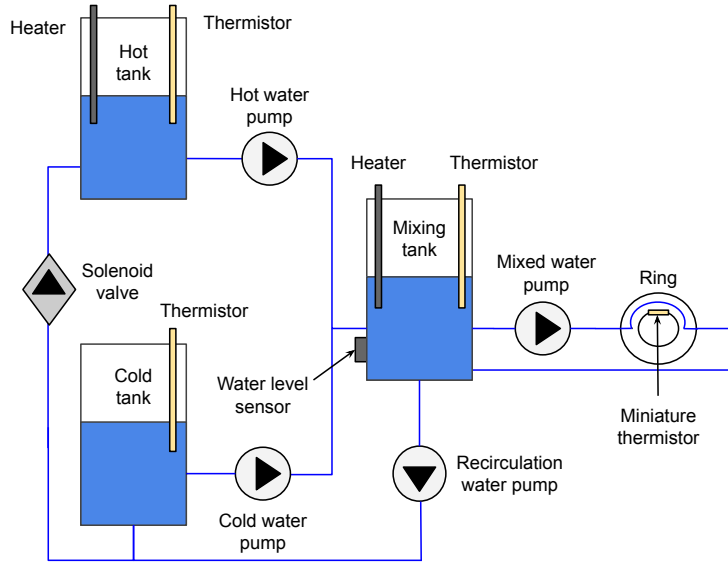


Figure 3: Schematic of the hydraulic circuit.

mixing tank was kept at a minimum to minimize delays by using a non-contact liquid level sensor (XKC-Y25-NPN), which triggered a hydraulic pump to return excess water to the hot and cold tanks. A solenoid valve (ADA-997, Adafruit) prevented backflow and unintended mixing between tanks. Additionally, a 100 W submersible heating element (860-7163, RS PRO) in the mixing tank activated when the temperature dropped below a set threshold, further reducing waiting times.

Water temperatures in the hot, cold, and mixing tanks were continuously monitored using submersible NTC thermistors (B57861S0103F040, EPCOS). To ensure accurate user-experienced temperature control, a miniature NTC thermistor (GA10K3MBD1, TE Connectivity) was positioned between the silicone tube and the ring, measuring the external surface temperature of the hydraulic tube.

The entire system is controlled by an Arduino Mega microcontroller. Dual H-bridge motor drivers (L298N, Kiwi Electronics) power and independently control the hydraulic pumps, linear actuator, and pneumatic valves. Meanwhile, each heating element is regulated by a relay module, ensuring safe and independent operation. While the pneumatic components are managed by directly toggling their activation states, the hydraulic system is regulated by a proportional controller. This controller dynamically adjusts pump speeds based on the difference between the target display temperature and the measured value to ensure precise temperature control.

2.3. Action-Based Texture Rendering

Beyond introducing our novel soft haptic ring, we present a data-driven, action-based rendering methodology for generating multimodal textures. This approach dynamically displays the most perceptible texture modalities based on users' exploratory actions. Prior research by Lederman and Klatzky (1987) identified distinct exploratory strategies for perceiving tactile properties, such as sliding for surface roughness, pressing for softness, and static contact for thermal cues. Our methodology leverages these natural interactions to selectively render each modality while considering the capabilities of our custom device (see Figure 4).

Using this approach, we aimed to replicate the experience of exploring surfaces with bare fingers by actuating the proximal phalanx through the ring device. We utilized the SENS3 database by Balasubramanian et al. (2025) to evaluate our device and methodology's rendering performance. This database includes multimodal tactile interaction data from participants exploring fifty surfaces with bare fingers using four exploratory procedures: static contact, pressing, tapping, and sliding. It also contains high-resolution top-view surface images and auditory recordings of interaction sounds.

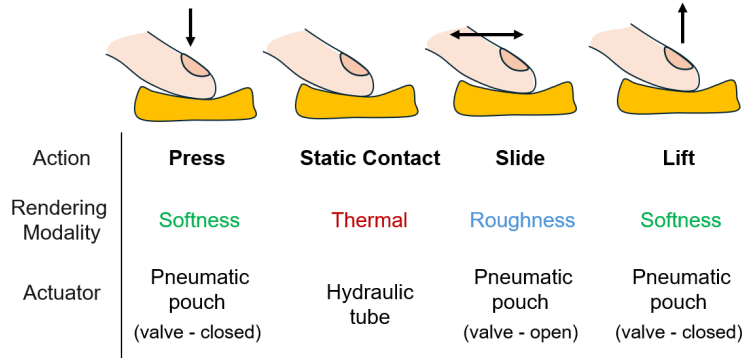


Figure 4: Rendering modalities and actuation mechanisms of the soft haptic ring in the proposed action-based rendering methodology.

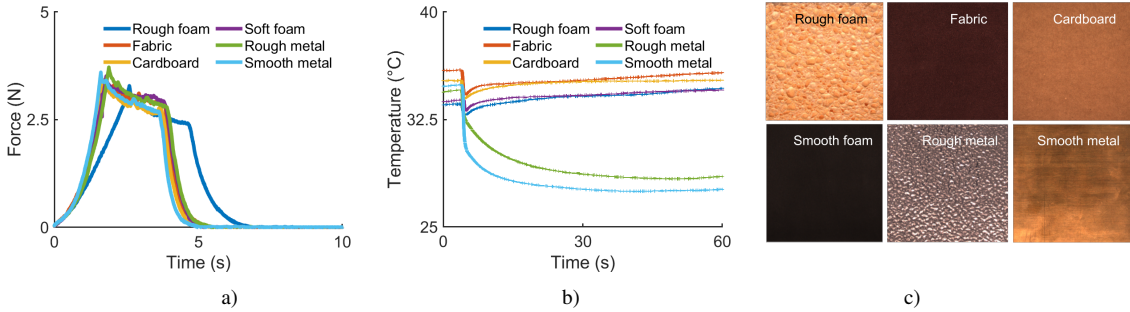


Figure 5: The texture data used from SENS3 Database (Balasubramanian et al., 2025). a) Pressing force as a function of time used for softness rendering. b) Skin temperature over time used for thermal rendering. c) Top view images of surfaces used for roughness rendering.

Although the SENS3 database includes high-fidelity finger-surface interaction recordings, the limitations of fluidic actuators prevented us from directly reproducing these signals. Instead, we aimed to generate a range of texture sensations that mimic real-world textures rather than achieving precise one-to-one rendering. Below, we describe how we processed these recordings to render sensations of softness, temperature, and roughness, along with the specific limitations of our device for each type of rendering.

Softness Rendering (Press & Lift Action):

The softness of an object is typically associated with perceived resistive and deformation cues, producing both kinesthetic and cutaneous sensations when force is applied (Srinivasan and LaMotte, 1995). Traditionally, object softness has been rendered using force-feedback devices, which dynamically modulate the displayed force (F) based on the depth of indentation (d) and the desired spring constant (k), following the linear relationship of $F = kd$ (Srinivasan and Basdogan, 1997). Recent works (Scilingo et al., 2010; Mete et al., 2024) have also proposed new haptic devices that can modulate resistance and deformation cues by independently controlling the stiffness and finger contact area.

As Section 2.1 explains, we render softness by applying pressure cues via the pneumatic pouch, which the linear actuator regulates when the connecting solenoid valve is closed. The applied air pressure modulates both resistance and deformation cues on the skin as the balloon-like pouch expands and contracts in response to pressure changes. We programmed the displacement of the linear actuator to render material softness.

The SENS3 database contains force sensor recordings of participants pressing materials with their index fingers while mounted on a linear stage. During each pressing action, the linear stage moved vertically at a constant speed (2 mm/s) until the applied force reached 3 N. Hence, pressing softer materials with lower stiffness took longer to reach the target force. In contrast, the maximum force was reached quickly when pressing on stiff materials. Figure 5a shows the measured pressing and lifting data in the SENS3 database for selected surfaces.

We leveraged these force profiles to render softness by calculating the pressing rate from the recorded data and mapping it to the actuator’s inflation speed. The moment of peak force in each signal was identified as the transition from the pressing phase to static contact. Using these profiles, we computed the pressing slope for each texture and mapped it to the actuator’s speed range, enabling dynamic inflation rates for a more realistic softness rendering.

In this approach, materials with a lower pressing slope—indicating softness—correspond to slower inflation speeds and lower applied forces. Conversely, stiffer materials with steeper pressing slopes inflate more quickly, generating stronger forces. A similar procedure was used to determine deflation speed by identifying the point at which the applied force decreased, signaling finger lift-off. Softer materials deflated more gradually, while stiffer ones deflated more abruptly.

As a result, the rendering signal follows a trapezoidal profile (see Figure 6a), where the rising and falling slopes correspond to the actuator’s inflation and deflation speeds, respectively. During the static contact phase, the rendering signal forms a plateau, maintaining a constant applied force. While the actual pressing signals in the database exhibit a slight decrease in force during this interval, we opted to simplify our model due to the limited controllability of our syringe-linear actuator setup. The actuator remains inflated and provides a steady force by keeping the linear actuator stationary during this phase.

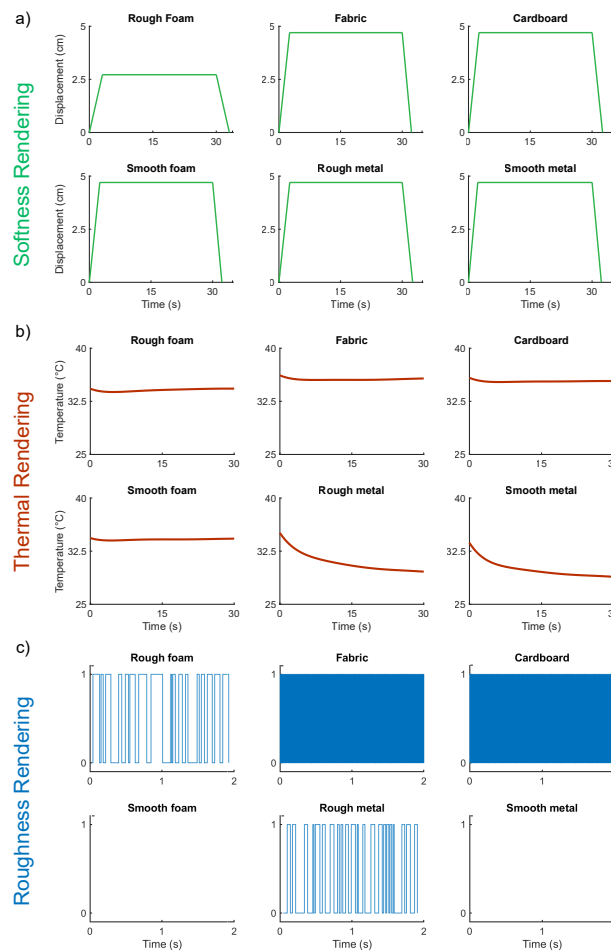


Figure 6: The signals sent to our soft haptic ring to render the selected textures. a) Displacement of the linear actuator connected to the pneumatic pouch for softness rendering. b) Display (hydraulic tube) temperatures for thermal rendering. c) Binary valve (fast switching solenoid) operation commands for roughness rendering. While the roughness rendering lasted 10 seconds during the experiments, only the first 2 seconds of the data are visualized for clarity.

Thermal Rendering (Static Contact Action):

Our perception of an object’s temperature—whether warm or cool—depends on the change in skin temperature caused by heat transfer between the object and our skin, which activates thermoreceptors within the skin. Typically, the temperature of the hand varies between 25 C° and 36 C° (Verrillo et al., 1998). Hence, when one touches an object at room temperature (20-22 C°), heat transfer from the skin to the object occurs. The change in the skin’s temperature at the contact point depends on the initial temperature of the skin and the material and the thermal properties of the material (Klatzky et al., 2013).

Rendering of thermal response between the skin and an object is typically achieved by modeling and replicating the heat transfer between the skin and the desired object. Many models have been proposed in the literature in the last century, and details of these can be found in the reviews by Johnson et al. (1979) and Jones and Ho (2008). In those models, the contact with skin and material is considered stationary.

We used the semi-infinite body model proposed by Ho and Jones (2006, 2008) to render thermal cues replicating the resulting heat transfer between the skin and a surface. Simulating object-skin interaction temperatures with a thermal display using this model requires knowledge of the skin temperature upon contact, the heat flux, and the thermal contact resistance between the skin and the display. We used recorded skin temperature and heat flux data during static contact with materials in the SENS3 database for the first two; see Figure 5b for measured skin temperatures for selected textures. We estimated the contact resistance of the designed display, the silicone tube embedded in the ring, as $0.0015 \text{ m}^2\text{K/W}$ (Intertronics, 2007). See Appendix A for more details on implementing the semi-infinite body model.

We pre-processed the skin temperature and heat flux data by applying a 10 Hz and a 1 Hz low-pass filter, respectively, to remove high-frequency noise. Next, we discarded the initial seconds of data when the finger had not yet made contact with the surface, as the model is only valid during skin-object interaction. These computations allowed us to determine the display temperature, which was then used by our control algorithm (see Figure 6b). To reduce data length and complexity, we fit a seventh-order polynomial to the display temperature curve before sending it to the microcontroller, which actuated the hydraulic circuit, pumping water through the tube to reproduce the required thermal profiles. We synchronized the thermal rendering with the static contact action. The temperature of the ring was kept constant during sliding action, as previously shown that humans cannot discriminate the surface temperature when they actively explore the surface (Green, 2010; Peters et al., 2023).

Roughness Rendering (Slide Action):

The perceived roughness of objects is influenced by skin deformations when pressed against surfaces, as well as vibrations and stretch when the skin moves across them (Weber et al., 2013). Various methodologies and haptic devices have been proposed in the literature to render surface roughness. One common approach captures and models interaction signals (forces or accelerations) from real surfaces in the frequency domain (e.g., via Fourier transform) and reproduces them using vibrotactile or surface haptic devices (Romano and Kuchenbecker, 2012; Fiedler and Vardar, 2019). Another method modulates interaction forces or vibrations by computing local gradients of a grayscale image of the surface (Basdogan et al., 1997; Kim et al., 2013). While the first approach enhances realism by incorporating contact interactions, the second effectively conveys surface topography.

Given the bandwidth constraints of our actuator (maximum 300 Hz) and the shift in stimulation location from the fingerpads to the finger phalanx, we adopted an image-based approach to render surface roughness. Our method combines an intensity-based algorithm with a peak detection function applied to high-resolution surface images. This approach leverages the relationship between surface texture and intensity variation: smoother textures exhibit more uniform intensities, while rougher textures show greater variance due to features such as bumps and creases.

To implement this method, we first applied a mean filter to grayscale surface images, reducing noise and eliminating high-frequency components that our valve cannot reproduce. Next, assuming uniform texture distribution, we extracted a one-dimensional signal by selecting a horizontal line of pixels at the texture’s mid-height. We then employed MATLAB’s `findpeaks` function (MathWorks, 2024) to analyze the signal’s relative intensity fluctuations. This function identified local maxima and minima based on neighboring values, enforcing a minimum separation distance aligned with the valve’s operating frequency. Peaks were selected based on their prominence (height relative to surrounding values), where local maxima indicated deactivation points for the valve, and local minima signaled activation.

The algorithm’s output was a binary square wave (see Figure 6c), structured according to pixel positions. To translate this into a time-based control signal, we applied a conversion factor of 50 mm/s—a speed chosen to balance dynamic exploration while operating within the valve’s limitations.

Despite the advantages of our peak detection algorithm, it has limitations when processing surfaces with very high-frequency textures, such as fabrics or cardboard. These textures produce intensity signals with small, densely packed peaks that the algorithm may fail to distinguish effectively, leading to an overestimation of roughness. To address this issue, we manually adjusted the square wave frequencies for these fine textures, capping them at the valve’s maximum operating frequency to ensure accurate rendering within the system’s constraints.

2.4. User Study

The user study aimed to assess the effectiveness of our haptic ring and texture rendering methodology in simulating the multimodal properties of real textures.

Participants:

Five women and ten men with an average age of 25.33 years (standard deviation, SD: 2.18) participated in the user study. Only one participant was left-handed. None of them presented any visual or sensory-motor disabilities. Regarding ring size, only one participant used the small-sized ring, five used the medium-sized ring, and nine employed the large-sized ring. The experimental protocol was approved by the TU Delft Human Research Ethics Committee (approval number 4546). All participants gave their informed consent.

Stimuli:

Our stimuli consisted of six textures—rough metal, smooth metal, rough foam, smooth foam, cardboard, and fabric—selected from the SENS3 database (Figure 5) and their virtual counterparts generated via the explained rendering methodology (Figure 6). These textures were chosen for their distinct thermal, roughness, and softness properties, aligning with our device’s actuation capabilities along these perceptual dimensions. The selection was guided by the reported principal component and factor loading analysis results of the adjective rating experiment conducted by Balasubramanian et al. (2025) across the 50 textures in the database. Figure B.11 visualizes the distribution of these textures in the perceptual space after the principal component and factor loading analysis.

Experimental Setup:

Each participant sat in front of a monitor and a set of six textures during the experiment; see Figure 7. Each texture was enclosed and hidden from the participant’s view by a custom 3D-printed case. The cases had openings covered by a plastic layer obscuring the textures visually while allowing participants to explore them freely by touch. Each box was labeled with a number from one to six to facilitate texture selection. Participants provided their responses through a graphical user interface (GUI) displayed on the monitor, using a computer mouse to interact with the system.

Participants wore the custom-designed soft ring on their dominant hand’s proximal phalanx of the index finger. For added comfort, they could rest their dominant arm on an armrest positioned in front of the textures. Throughout the experiment, users wore noise-canceling headphones (W830NB, Edifier) that played white noise to block auditory cues and minimize distractions.

Experimental Procedure:

Our experiments consisted of two tasks: a rating task and a matching task. In the rating task, participants rated the perceived sensations of presented textures (real or virtual) using the adjective pairs flat–bumpy, cold–hot, and soft–stiff. These pairs were selected as they are commonly used in the literature to represent texture’s roughness, thermal, and softness dimensions (Okamoto et al., 2013). In the matching task, participants matched the virtual textures experienced through the ring with the six selected real textures.

Before the experiments began, each participant thoroughly washed their hands. Then, they were briefed about the study and asked to explore each physical texture using their dominant hand’s index finger. When exploring the surfaces, they were asked to apply the press, static contact, and sliding actions (not necessarily consecutively). During this process, participants were presented with a graphical user interface (GUI), where they were asked to rate each texture based on flat-bumpy, cold-hot, and soft-stiff adjective pairs using the sliders displayed on the GUI. Each slider

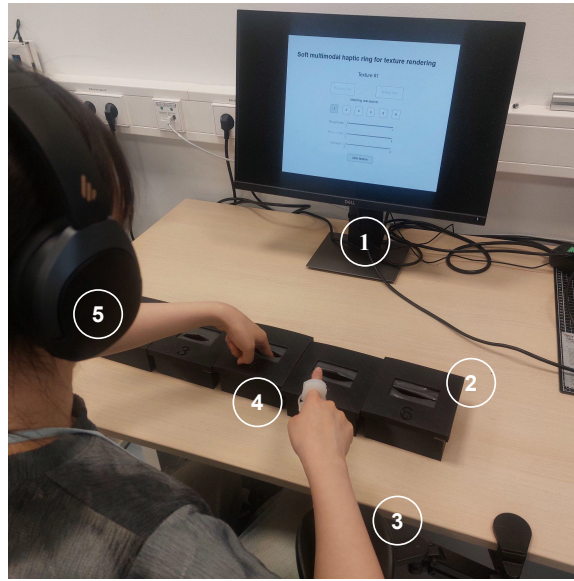


Figure 7: Experimental setup: (1) monitor displaying GUI, (2) textures within the 3D-printed enclosure, (3) armrest, (4) soft multimodal haptic ring, (5) noise-canceling headphones

had 100 increments for each adjective pair. They were allowed to switch between the textures and explore them as much as they wanted. They were instructed to rate the textures considering only the six textures they were presented.

After completing the first adjective rating stage, participants wore the multimodal ring on the index finger of their dominant hand. The experimenter ensured the proper placement of the actuators and the secure positioning of the sensing elements. The second part of the experiment commenced once participants were familiar with the setup. During this stage, participants were asked to interact with a GUI displaying two actions: press-wait-lift and slide. The press-wait-lift action simulated pressing and maintaining static contact with a surface for 30 seconds, while the slide action simulated the lateral exploration of a surface at a speed of 50 mm/s for 10 seconds. The GUI displayed a virtual ball moving at the corresponding rates and directions to guide participants' exploratory action. For the sliding action, the ball moved horizontally, while for the pressing action, the ball moved vertically, descending and then remaining stationary to represent static contact. The participants were instructed to mimic these movements with their ring-equipped index finger. They were also encouraged to continue exploring the real textures with their non-dominant hand as much as needed throughout the experiment.

Participants were instructed to start every texture trial with the slide action. Upon pressing the corresponding button in the GUI, a five-second countdown began, followed by the appearance of the moving ball on the screen and the start of the roughness simulation. After completing the sliding simulation, participants proceeded to the press-and-wait action, where temperature and pressure cues were provided simultaneously. For this action, the countdown did not start immediately after pressing the button. Instead, a "preparing" label appeared on the screen to indicate a preparation stage, during which the water and ring tube display were heated to the required initial temperature. Once this temperature was reached, the five-second countdown began, followed by the appearance of the moving ball on the screen.

After completing both actions, participants were asked to select the real surface that best matched the virtual texture. They also rated the perceived virtual stimuli using the previously mentioned adjective pairs. Both tasks were completed directly through the GUI. After submitting their responses, participants continued to the next texture, for which the same approach was repeated. In total, four rounds were conducted, displaying each texture once per round and accounting for a total of twenty-four trials per participant. The order of the displayed textures was randomized for each round. The first round was considered the training phase. Hence, the participant responses from this phase were excluded from the analysis.

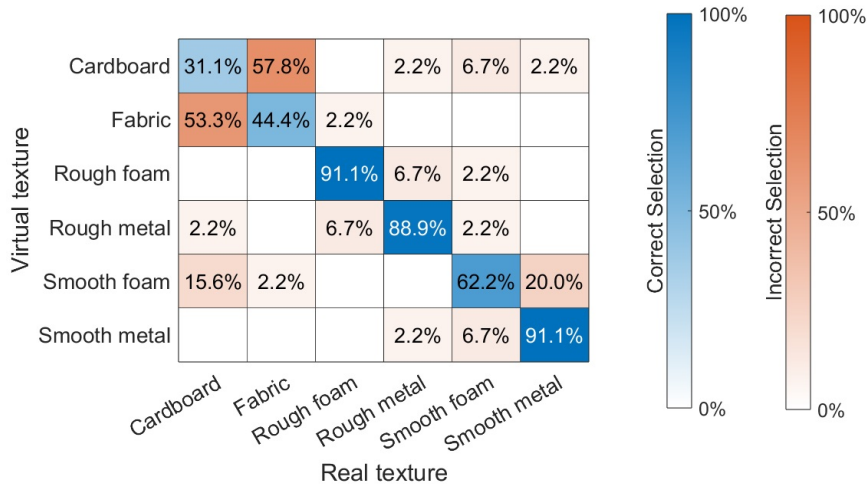


Figure 8: The confusion matrix for the matching task displays the presented virtual textures as rows and the selected real textures as columns. Each cell indicates the proportion of times a given pair was chosen, with the diagonal representing the expected correct answers.

3. Results

The matching percentage between the virtual textures displayed by the ring and the real surfaces selected by the participants is shown in Figure 8. In this analysis, each participant’s responses across the three rounds were treated as independent data points rather than being averaged. A two-sample Pearson Chi-Squared test ($\chi^2(25, N = 270) = 756, p < 0.001$) indicated that the distribution of participant predictions significantly deviates from the expected chance level (1/6 probability per texture).

Figure 9 presents the adjective ratings of virtual textures compared to their real counterparts in terms of perceived roughness, temperature, and softness. Since the rating tasks for real and virtual textures were conducted in separate experiments, this figure offers insights into the device’s rendering performance across different textures rather than serving as a direct one-to-one comparison.

Additionally, we assessed the device’s performance in rendering various texture sensations. A Kolmogorov-Smirnov test was first conducted to determine the normality of each distribution, revealing significant deviations from normality ($p < 0.05$). As a result, a Kruskal-Wallis test was performed to identify statistically significant differences in adjective ratings across textures and modalities. The results of this analysis are presented in Figure 10 for roughness, temperature, and softness, respectively, for both real and virtual textures.

4. Discussion

In this paper, we presented a soft, wearable haptic device capable of delivering vibration, pressure, and temperature stimuli to the user’s proximal phalanx. Additionally, we introduced an action-based rendering approach for displaying multimodal textures through our device. We conducted a user study to evaluate the effectiveness of both the device and rendering method in conveying texture sensations. Participants matched the displayed virtual textures to their real counterparts and rated the perceived sensations of both real and virtual textures.

The results of the matching task indicate that participants were able to associate the virtual textures displayed by the haptic ring with their real counterparts, as the correct matching rate for all textures was significantly higher than the chance level (see Figure 8). The rough foam, rough metal, and smooth metal textures achieved the highest accuracy, reaching 90%. Interestingly, these textures also exhibited the adjective ratings at utmost margins among the selected surfaces, likely due to their distinct characteristics—such as the pronounced temperature contrast of metals, the bumpy texture of rough foam and rough metal, or the softness of rough foam. These are visible both in our experiments (Figure 9) and perceptual space found by Balasubramanian et al. (2025).

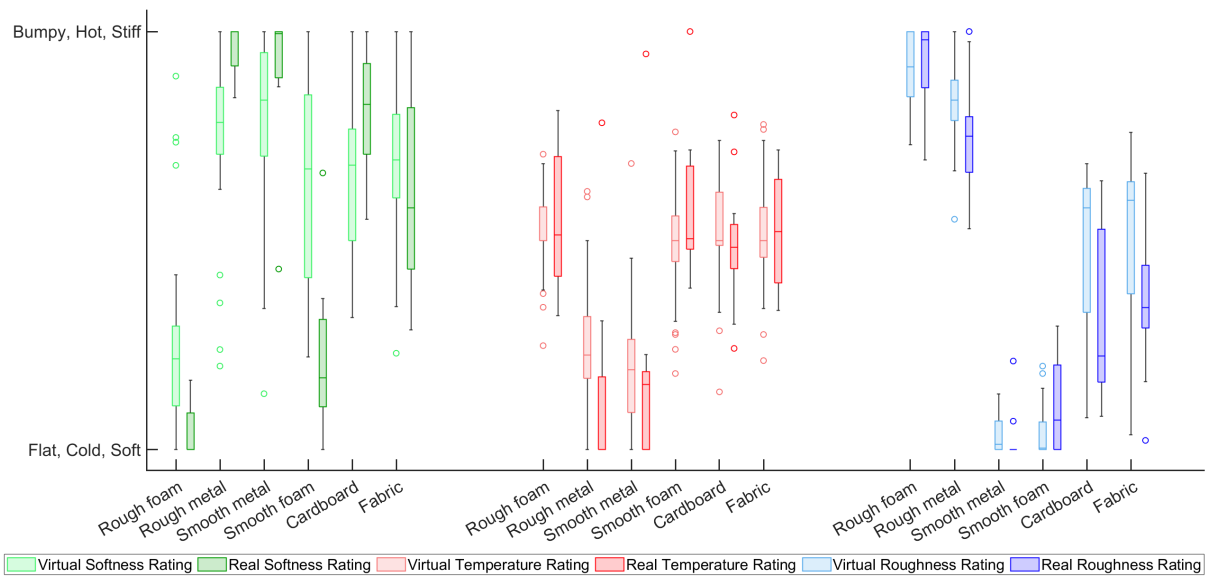


Figure 9: Comparison between adjective ratings for the soft ring-displayed virtual textures (light) and the real freely explored textures (dark), for their roughness, temperature, and softness dimensions.

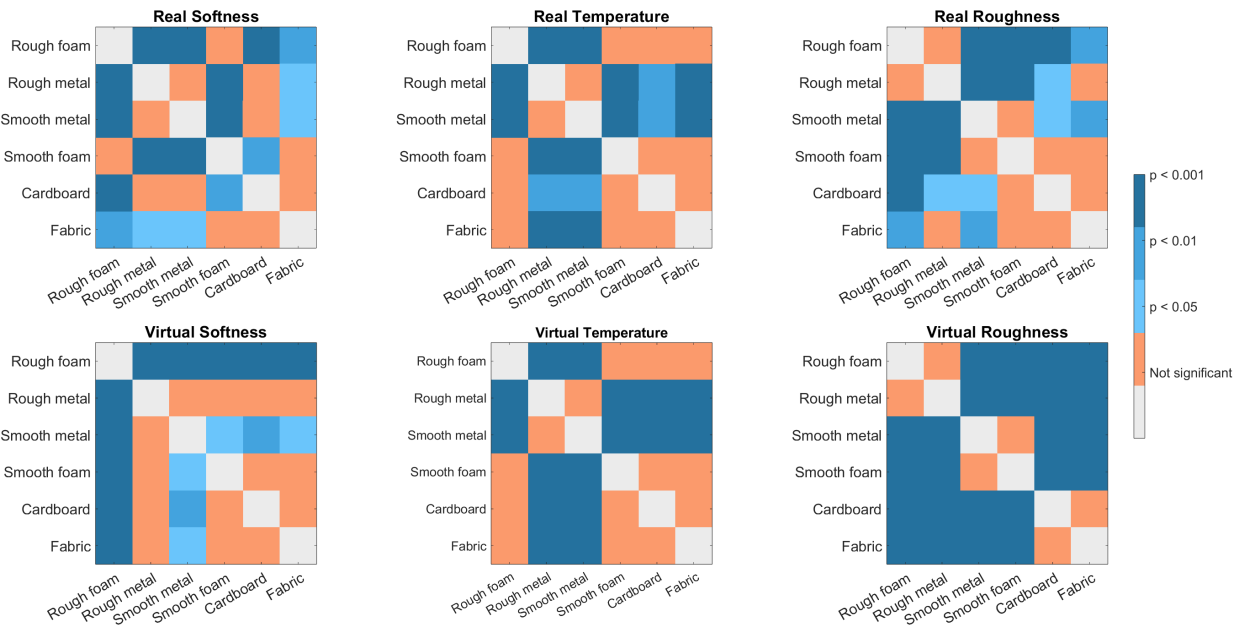


Figure 10: Results of the Kruskal-Wallis test on perceived differences in the roughness, temperature, and softness dimensions. The upper row presents the results for the real textures, while the lower row shows the results for the displayed virtual textures.

Smooth foam, with a correct identification rate of 62.2%, was often misclassified as smooth metal or cardboard. This lower accuracy may stem from its perceived roughness, which is similar to smooth metal, or its temperature, which resembles that of cardboard (see Figures 9 and 10). Furthermore, the virtual smooth foam's perceived softness was less distinctive than its real counterpart, potentially contributing to the misclassification. Fabric and cardboard textures yielded the poorest matching results, with correct identification rates below 50%. While participants could

recognize that the displayed texture belonged to one of these two categories, distinguishing between them was largely a matter of chance. This outcome was expected, given their highly similar profiles across all dimensions, both in the rendering and the real texture-recorded signals (Figure 5), and the adjective ratings (Figure 10).

Adjective ratings of virtual and real textures revealed varying sensations of roughness, temperature, and softness (see Figures 9 and 10). Regarding softness, only rough foam was rated as very soft, while all other textures were considered relatively stiff. Smooth metal, identified as the stiffest real texture, was also rated as the stiffest virtual texture in our adjective assessments. For temperature, two distinct levels emerged: cold and medium. Metals stood out with their colder temperature profile, while all other materials were perceived as having similar, near-room-temperature warmth. Roughness fell into three distinct levels: rough foam and rough metal were perceived as very bumpy, smooth foam and smooth metal as very flat, and fabric and cardboard as moderately rough. This pattern aligns with the matching task results, where textures with similar roughness—such as cardboard and fabric or smooth foam and smooth metal—were frequently confused.

When comparing adjective ratings of our virtual textures to those of real textures, the temperature dimension exhibited the highest similarity among all dimensions (see Figure 10). Using our soft ring, we successfully generated virtual textures that closely mirrored the thermal differences observed in their corresponding real textures. These results suggest that our temperature rendering approach was the most accurate, which is unsurprising given that the rendering algorithm by Ho and Jones (2008) has been extensively studied. Moreover, the high sensitivity to cold and warm stimuli on the dorsal side of the hand, where the thermal stimuli were applied, may have contributed to these results (Wakolbinger et al., 2014).

In contrast, our ring’s ability to render softness and roughness was more limited. For softness, only rough foam and smooth metal were perceived as significantly different from the other textures. Interestingly, for roughness, texture differences were more pronounced with our ring compared to the real textures. We believe these results stem from the simplified softness and roughness rendering methods imposed by the constraints of our pneumatic actuator. The limited information we could convey through pressure and vibration may have contributed to these findings. For instance, when participants pressed real surfaces, they received cutaneous and kinesthetic cues. However, only the former was available for the virtual textures. The absence of kinesthetic information may have influenced perceived softness variations (Dhong et al., 2019; Srinivasan and LaMotte, 1995). Additionally, for roughness, our limited ability to render variations in amplitude and friction—both of which contribute to perceived roughness (İşleyen et al., 2020; Friesen et al., 2021; Richardson et al., 2022)—may have led to exaggerated differences in the virtual textures.

Overall, our results underscore the critical role of multimodality in surface perception, as reflected in both the matching and rating task results. In post-experimental discussions, participants emphasized the necessity of experiencing all three haptic modalities to accurately match perceived cues to real textures, noting that omitting any modality would have significantly increased the difficulty. Specifically, our experiment highlighted the importance of thermal cues, with many participants relying more on temperature stimuli than softness cues. Notably, those who perceived thermal cues less clearly described the simulation as less realistic. This was particularly evident in one participant with a small scar near the temperature-sensing area, who experienced the task more as “pattern matching” than a texture simulation.

Additionally, our findings demonstrate that haptic cues can be effectively relocated from the fingertip to the phalanx. The successful texture matching with notable accuracy supports the feasibility of transferring haptic cues from the fingertip to other parts of the finger. These results are consistent with previous studies, which showed that humans can successfully differentiate texture information through a ring display (Gaudeni et al., 2019; Friesen and Vardar, 2024; Normand et al., 2025).

Despite a careful design process, our device had some limitations. While we produced rings in three sizes to accommodate various finger types, the fit was not always perfect. Some participants found them slightly too tight or loose, potentially affecting the perception of displayed cues (Pra et al., 2023; Galie et al., 2009). Additionally, despite efforts to maintain consistent inflation characteristics across all rings, minor variations in the manufacturing process may have introduced slight differences in performance. Furthermore, although our ring was wearable, soft, small, lightweight, and flexible, it required large, complex, and bulky circuits to operate, significantly restricting its usability and application. Despite our encouraging results, we believe that simplifying the system is essential, even if it is to the detriment of our design’s soft and flexible character. As such, we recommend future versions of the system to replace the hydraulic circuit with a Peltier cell that provides thermal cues. We recommend enclosing this element within a silicone layer to reduce its stiffness and integrate better within the ring. Alternatively, flexible thermal interfaces, such

as the one developed by Lee et al. (2020), which combines heating and cooling functions while maintaining softness, could be used. Additionally, for a more compact version of the device, we suggest replacing the air compressor with a portable system based on small air cartridges, as illustrated by Talhan et al. (2020). We believe these modifications would lead to a more wearable system with improved control, enhancing its applicability and practicality.

5. Conclusions

In this work, we present a novel wearable haptic device and a rendering methodology designed to deliver multimodal texture sensations while allowing users to interact with their physical surroundings using their bare fingers. To the best of our knowledge, this is the first soft, multimodal haptic ring capable of independently providing pressure, thermal, and vibratory stimuli. Our system has successfully demonstrated the ability to simulate real textures' thermal, roughness, and compliance properties with up to 90% accuracy, effectively rendering distinct cues across all three perceptual dimensions.

The presented haptic ring and rendering methodology holds great potential for future applications, particularly in mixed and augmented reality. A multimodal wearable interface that delivers realistic haptic simulations while allowing unrestricted movement and natural exploration of virtual environments could mark a transformative advancement in haptic technology.

6. Data availability

The data and codes used in this paper will be publicly available upon acceptance.

7. Acknowledgements

This work was partly funded by the Dutch Research Council (NWO) with projects 19153 and OCENW.XS23.1.178. The authors also thank Jagan K. Balasubramanian for helping with the use of the SENS3 database, Haewon Jeong for fabricating soft materials, and Khoa Lahn for his help in thermal rendering.

8. CRediT authorship contribution statement

Ana Sanz Cozcolluela: Conceptualization, Methodology, Software, Formal Analysis, Investigation, Writing - Original Draft, Writing - Review & Editing, and Visualization. **Yasemin Vardar:** Conceptualization, Methodology, Formal Analysis, Writing - Original Draft, Writing - Review & Editing, Visualization, Supervision, and Funding Acquisition.

9. Declaration of competing interest

The authors declare they have no known competing financial interests or personal relationships that could have influenced this work.

10. Declaration of generative AI and AI-assisted technologies in the writing process

The authors used OpenAI's ChatGPT and Grammarly Inc.'s Grammarly tool to enhance the language and readability of this work. After using these tools, the authors carefully reviewed and edited the content as needed. They take full responsibility for the final publication.

Appendix A. Implementation of semi-infinite body model

The semi-infinite body model proposed by Ho and Jones (2006, 2008) considers that the thermal interaction between the skin and the material with which it is in contact is a transient process dominated by heat conduction. In this process, heat is transferred across the interface and flows through a thermal contact resistance. Consequently, during contact, the heat flux of the skin and that of the material will be identical, where the flux is determined by the difference between the skin surface temperature and the object surface temperature divided by the thermal contact resistance. This relationship is described by Equations A.1 and A.2, where $q''_{skin,s}$, $q''_{object,s}$, $T_{skin,s}$ and $T_{object,s}$ refer to the heat flux and temperature of the skin and object surfaces, respectively, and $R_{skin,object}$ stands for the thermal contact resistance between skin and object.

$$q''_{skin,s} = q''_{object,s} = q'' \quad (A.1)$$

$$q'' = \frac{T_{skin,s}(t) - T_{object,s}(t)}{R_{skin,object}} \quad (A.2)$$

Thermal contact resistance depends on several variables related to the thermal and mechanical properties of the contacting surfaces. For materials with an even surface and interaction contact forces around 2 N, it can be approximated by Equation A.3, where k_{object} is the thermal conductivity of the object.

$$R_{skin,object} = \frac{0.37 + k_{object}}{1870 \cdot k_{object}} \quad [m^2 K/W] \quad (A.3)$$

The semi-infinite body model can be further extended to predict the temperature at which a thermal display should be activated to reproduce the thermal characteristics of an object in contact with the skin (Jones and Ho, 2008). This can be done simply by replacing the object terms of the previous equations with those of the display:

$$q'' = \frac{T_{skin,s}(t) - T_{object,s}(t)}{R_{skin,object}} = \frac{T_{skin,s}(t) - T_{display}(t)}{R_{skin-display}} \quad (A.4)$$

$$T_{display}(t) = T_{skin,s}(t) \cdot \left[1 - \frac{R_{skin,display}}{R_{skin,object}}\right] + \frac{R_{skin,display}}{R_{skin,object}} \cdot T_{object,s}(t) \quad (A.5)$$

These equations, when combined with Equation A.2, yield an expression that allows us to compute $T_{display}$ as a function of the heat flux and the thermal contact resistance between the skin and thermal display:

$$T_{display}(t) = T_{skin,s}(t) - q'' \cdot R_{skin-display} \quad (A.6)$$

Appendix B. Texture Selection

We selected six textures from the SENS3 database based on the analysis conducted by (Balasubramanian et al., 2025). In their experiments, participants interacted with 50 surfaces and rated their psychophysical sensations. Then, they used principal component analysis (PCA) to analyze the adjective ratings. From the analysis, they chose four dimensions that represented 95% of the total variance. Following this, they did factor analysis through varimax rotation of the component matrix. Figure B.11 visualizes the locations of the selected surfaces in the perceptual space.

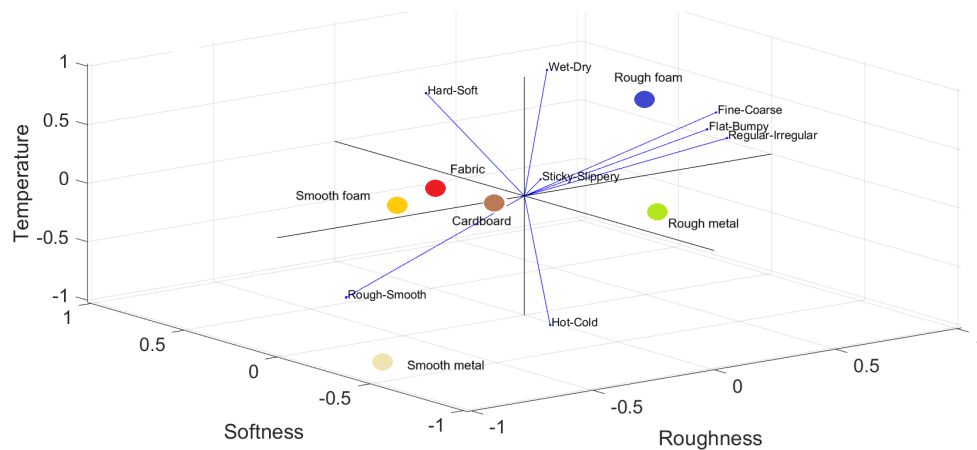


Figure B.11: The locations of the selected surfaces in the perceptual space which was obtained by applying principal component and factor loading analyses on the perceptual rating experiments conducted by Balasubramanian et al. (2025).

References

- Balasubramanian, J.K., Kodak, B.L., Vardar, Y., 2025. Sens3: Multisensory database of finger-surface interactions and corresponding sensations, in: Kajimoto, H., Lopes, P., Pacchierotti, C., Basdogan, C., Gori, M., Lemaire-Semal, B., Marchal, M. (Eds.), *Haptics: Understanding Touch: Technology and Systems; Applications and Interaction*, Springer Nature Switzerland, Cham, pp. 262–277.
- Basdogan, C., Ho, C.H., Srinivasan, M.A., 1997. A ray-based haptic rendering technique for displaying shape and texture of 3d objects in virtual environments, pp. 77–84. doi:10.1115/IMECE1997-0380.
- Biswas, S., Visell, Y., 2019. Emerging material technologies for haptics. *Advanced Materials Technologies* 4, 1900042. URL: <https://doi.org/10.1002/admt.201900042>.
- Dhong, C., Miller, R., Root, N.B., Gupta, S., Kayser, L.V., Carpenter, C.W., Loh, K.J., Ramachandran, V.S., Lipomi, D.J., 2019. Role of indentation depth and contact area on human perception of softness for haptic interfaces. *Science Advances* 5. URL: <http://dx.doi.org/10.1126/sciadv.aaw8845>, doi:10.1126/sciadv.aaw8845.
- El Saddik, A., 2007. The potential of haptics technologies. *IEEE Instrumentation & Measurement Magazine* 10, 10–17. doi:10.1109/MIM.2007.339540.
- Fiedler, T., Vardar, Y., 2019. A novel texture rendering approach for electrostatic displays., in: *International Workshop on Haptic and Audio Interaction Design - HAID2019*. doi:hal-02011782v3.
- Friesen, R.F., Klatzky, R.L., Peshkin, M.A., Colgate, J.E., 2021. Building a navigable fine texture design space. *IEEE Transactions on Haptics* 14, 897–906. doi:10.1109/TOH.2021.3092077.
- Friesen, R.F., Vardar, Y., 2024. Perceived realism of virtual textures rendered by a vibrotactile wearable ring display. *IEEE Transactions on Haptics* 17, 216–226. doi:10.1109/TOH.2023.3304899.
- Galie, J., Ho, H.N., Jones, L.A., 2009. Influence of contact conditions on thermal responses of the hand, in: *World Haptics 2009 - Third Joint EuroHaptics conference and Symposium on Haptic Interfaces for Virtual Environment and Teleoperator Systems*, pp. 587–592. doi:10.1109/WHC.2009.4810902.
- Gaudeni, C., Meli, L., Jones, L.A., Prattichizzo, D., 2019. Presenting surface features using a haptic ring: A psychophysical study on relocating vibrotactile feedback. *IEEE Transactions on Haptics* 12, 428–437. doi:10.1109/TOH.2019.2938945.
- Goetz, D.T., Owusu-Antwi, D.K., Culbertson, H., 2020. Patch: Pump-actuated thermal compression haptics, in: *2020 IEEE Haptics Symposium (HAPTICS)*, pp. 643–649. doi:10.1109/HAPTICS45997.2020.ras.HAP20.32.c4048ec3.
- Green, B.G., 2010. Temperature perception on the hand during static versus dynamic contact with a surface. *Attention, Perception, and Psychophysics* 71, 1185–1196. doi:10.3758/APP.71.5.118.
- Han, T., Anderson, F., Irani, P., Grossman, T., 2018. Hydroring: Supporting mixed reality haptics using liquid flow, pp. 913–925. doi:10.1145/3242587.3242667.
- Hashem, M.S., Joolae, J.B., Hassan, W., Jeon, S., 2022. Soft pneumatic fingertip actuator incorporating a dual air chamber to generate multi-mode simultaneous tactile feedback. *Applied Sciences* 12. URL: <https://www.mdpi.com/2076-3417/12/1/175>, doi:10.3390/app12010175.
- Ho, H.N., Jones, L., 2006. Thermal model for hand-object interactions, in: *2006 14th Symposium on Haptic Interfaces for Virtual Environment and Teleoperator Systems*, pp. 461–467. doi:10.1109/HAPTIC.2006.1627108.
- Ho, H.N., Jones, L.A., 2008. Modeling the thermal responses of the skin surface during hand-object interactions. *Journal of Biomechanical Engineering* 130. URL: <http://dx.doi.org/10.1115/1.2899574>, doi:10.1115/1.2899574.
- Intertronics, 2007. Thermally conductive silicones. <https://www.intertronics.co.uk/wp-content/uploads/2016/11/TB2007-12-Thermally-Conductive-Silicones.pdf>.
- Johnson, K.O., Darian-Smith, I., LaMotte, C., Johnson, B., Oldfield, S., 1979. Coding of incremental changes in skin temperature by a population of warm fibers in the monkey: correlation with intensity discrimination in man. *Journal of Neurophysiology* 42, 1332–1353. URL: <https://doi.org/10.1152/jn.1979.42.5.1332>.

- org/10.1152/jn.1979.42.5.1332, doi:10.1152/jn.1979.42.5.1332, arXiv:<https://doi.org/10.1152/jn.1979.42.5.1332>, PMID: 114610.
- Jones, L.A., Ho, H.N., 2008. Warm or cool, large or small? the challenge of thermal displays. *IEEE Transactions on Haptics* 1, 53–70. doi:10.1109/TOH.2008.2.
- Kalra, A.M., Lowe, A., Al-Jumaily, A.M., 2016. Mechanical behaviour of skin: A review. *Journal of Material Sciences & Engineering* 5, 1–7. URL: <https://api.semanticscholar.org/CorpusID:8773355>.
- Kim, S.C., Israr, A., Poupyrev, I., 2013. Tactile rendering of 3d features on touch surfaces, in: *Proceedings of the 26th Annual ACM Symposium on User Interface Software and Technology*, Association for Computing Machinery, New York, NY, USA. p. 531–538. URL: <https://doi.org/10.1145/2501988.2502020>, doi:10.1145/2501988.2502020.
- Klatzky, R.L., Pawluk, D., Peer, A., 2013. Haptic perception of material properties and implications for applications. *Proceedings of the IEEE* 101, 2081–2092. doi:10.1109/JPROC.2013.2248691.
- Kodak, B.L., Vardar, Y., 2023. Feelpen: A haptic stylus displaying multimodal texture feels on touchscreens. *IEEE/ASME Transactions on Mechatronics* 28, 2930–2940. doi:10.1109/TMECH.2023.3264787.
- Lederman, S.J., Klatzky, R.L., 1987. Hand movements: A window into haptic object recognition. *Cognitive Psychology* 19, 342–368. URL: <https://www.sciencedirect.com/science/article/pii/0010028587900089>, doi:[https://doi.org/10.1016/0010-0285\(87\)90008-9](https://doi.org/10.1016/0010-0285(87)90008-9).
- Lee, J., Sul, H., Lee, W., Pyun, K.R., Ha, I., Kim, D., Park, H., Eom, H., Yoon, Y., Jung, J., Lee, D., Ko, S.H., 2020. Stretchable skin-like cooling/heating device for reconstruction of artificial thermal sensation in virtual reality. *Advanced Functional Materials* 30. doi:10.1002/adfm.201909171.
- Liu, Y., Nishikawa, S., Seong, Y., Niiyama, R., Kuniyoshi, Y., 2021. Thermocaress: A wearable haptic device with illusory moving thermal stimulation, pp. 1–12. doi:10.1145/3411764.3445777.
- MathWorks, 2024. Find Local Maxima - MATLAB findpeaks. URL: <https://nl.mathworks.com/help/signal/ref/findpeaks.html>.
- Mete, M., Jeong, H., Wang, W.D., Paik, J., 2024. Sori: A softness-rendering interface to unravel the nature of softness perception. *Proceedings of the National Academy of Sciences* 121, e2314901121. URL: <https://www.pnas.org/doi/abs/10.1073/pnas.2314901121>, doi:10.1073/pnas.2314901121, arXiv:<https://www.pnas.org/doi/pdf/10.1073/pnas.2314901121>.
- Normand, E., Pacchierotti, C., Marchand, E., Marchal, M., 2025. Augmenting the texture perception of tangible surfaces in augmented reality using vibrotactile haptics, in: Kajimoto, H., Lopes, P., Pacchierotti, C., Basdogan, C., Gori, M., Lemaire-Semal, B., Marchal, M. (Eds.), *Haptics: Understanding Touch; Technology and Systems; Applications and Interaction*, Springer Nature Switzerland, Cham. pp. 469–484.
- Okamoto, S., Nagano, H., Yamada, Y., 2013. Psychophysical dimensions of tactile perception of textures. *IEEE Transactions on Haptics* 6, 81–93. URL: <http://dx.doi.org/10.1109/TOH.2012.32>, doi:10.1109/toh.2012.32.
- Pacchierotti, C., Salvietti, G., Hussain, I., Meli, L., Prattichizzo, D., 2016. The hring: A wearable haptic device to avoid occlusions in hand tracking, in: *2016 IEEE Haptics Symposium (HAPTICS)*, pp. 134–139. doi:10.1109/HAPTICS.2016.7463167.
- Pacchierotti, C., Sinclair, S., Solazzi, M., Frisoli, A., Hayward, V., Prattichizzo, D., 2017. Wearable haptic systems for the fingertip and the hand: Taxonomy, review, and perspectives. *IEEE Transactions on Haptics* 10, 580–600. doi:10.1109/TOH.2017.2689006.
- Peters, L., Serhat, G., Vardar, Y., 2023. Thermosurf: Thermal display technology for dynamic and multi-finger interactions. *IEEE Access* 11, 12004–12014. doi:10.1109/ACCESS.2023.3242040.
- Pra, Y.D., Papetti, S., Järveläinen, H., Bianchi, M., Fontana, F., 2023. Effects of vibration direction and pressing force on finger vibrotactile perception and force control. *IEEE Transactions on Haptics* 16, 23–32. doi:10.1109/TOH.2022.3225714.
- Rameshwar, R., Skorina, E.H., Onal, C.D., 2023. Fabric-silicone composite haptic muscles for sensitive wearable force feedback, Association for Computing Machinery, New York, NY, USA. p. 33–41. URL: <https://doi.org/10.1145/3594806.3594853>, doi:10.1145/3594806.3594853.
- Richardson, B.A., Vardar, Y., Wallraven, C., Kuchenbecker, K.J., 2022. Learning to feel textures: Predicting perceptual similarities from unconstrained finger-surface interactions. *IEEE Transactions on Haptics* 15, 705–717. doi:10.1109/TOH.2022.3212701.
- van Riessen, H.A.J., Vardar, Y., 2023. Relocating thermal stimuli to the proximal phalanx may not affect vibrotactile sensitivity on the fingertip. URL: <https://arxiv.org/abs/2312.07261>, arXiv:2312.07261.
- Romano, J.M., Kuchenbecker, K.J., 2012. Creating realistic virtual textures from contact acceleration data. *IEEE Transactions on Haptics* 5, 109–119. doi:10.1109/TOH.2011.38.
- Scilingo, E.P., Bianchi, M., Grioli, G., Bicchi, A., 2010. Rendering softness: Integration of kinesthetic and cutaneous information in a haptic device. *IEEE Transactions on Haptics* 3, 109–118. doi:10.1109/TOH.2010.2.
- Srinivasan, M.A., Basdogan, C., 1997. Haptics in virtual environments: Taxonomy, research status, and challenges. *Computers & Graphics* 21, 393–404. URL: <https://www.sciencedirect.com/science/article/pii/S0097849397000307>, doi:[https://doi.org/10.1016/S0097-8493\(97\)00030-7](https://doi.org/10.1016/S0097-8493(97)00030-7). haptic Displays in Virtual Environments and Computer Graphics in Korea.
- Srinivasan, M.A., LaMotte, R.H., 1995. Tactile discrimination of softness. *Journal of neurophysiology* 73 1, 88–101. URL: <https://api.semanticscholar.org/CorpusID:22017465>.
- Sun, Z., Zhu, M., Shan, X., Lee, C., 2022. Augmented tactile-perception and haptic-feedback rings as human-machine interfaces aiming for immersive interactions. *Nature Communications* 13. URL: <http://dx.doi.org/10.1038/s41467-022-32745-8>, doi:10.1038/s41467-022-32745-8.
- Talhan, A., Kim, H., Jeon, S., 2020. Tactile ring: Multi-mode finger-worn soft actuator for rich haptic feedback. *IEEE Access* 8, 957–966. doi:10.1109/ACCESS.2019.2961430.
- Talhan, A., Kumar, S., Kim, H., Hassan, W., Jeon, S., 2022. Multi-mode soft haptic thimble for haptic augmented reality based application of texture overlaying. *Displays* 74, 102272. URL: <https://www.sciencedirect.com/science/article/pii/S0141938222000920>, doi:<https://doi.org/10.1016/j.displa.2022.102272>.
- Teng, S.Y., Lopes, P., 2022. Xr needs “mixed feelings”: engineering haptic devices that work in both virtual and physical realities. *XRDS* 29, 44–47. URL: <https://doi.org/10.1145/3558194>, doi:10.1145/3558194.
- Verrillo, R., Bolanowski, S., Francis, C., Mcglone, F., 1998. Effects of hydration on tactile sensation. *Somatosen-*

- sory & Motor Research 15, 93–108. URL: <https://doi.org/10.1080/08990229870826>, doi:10.1080/08990229870826, arXiv:<https://doi.org/10.1080/08990229870826>.
- de Vlam, V., Wiertelwski, M., Vardar, Y., 2023. Focused vibrotactile stimuli from a wearable sparse array of actuators. *IEEE Transactions on Haptics* 16, 511–517. doi:10.1109/TOH.2023.3270362.
- Wakolbinger, R., Roche, A.D., Stockinger, T., Gustorff, B., Aszmann, O.C., 2014. Multiregion thermal sensitivity mapping of the hand. *Journal of Plastic, Reconstructive & Aesthetic Surgery* 67, 1541–1547. URL: <https://www.sciencedirect.com/science/article/pii/S1748681514003477>, doi:<https://doi.org/10.1016/j.bjps.2014.06.017>.
- Weber, A.I., Saal, H.P., Lieber, J.D., Cheng, J.W., Manfredi, L.R., Dammann, J.F., Bensmaia, S.J., 2013. Spatial and temporal codes mediate the tactile perception of natural textures. *Proceedings of the National Academy of Sciences* 110, 17107–17112. URL: <https://www.pnas.org/doi/abs/10.1073/pnas.1305509110>, doi:10.1073/pnas.1305509110, arXiv:<https://www.pnas.org/doi/pdf/10.1073/pnas.1305509110>.
- Zhang, B., Sra, M., 2021. Pneumod: A modular haptic device with localized pressure and thermal feedback, in: *Proceedings of the 27th ACM Symposium on Virtual Reality Software and Technology*, Association for Computing Machinery, New York, NY, USA. URL: <https://doi.org/10.1145/3489849.3489857>, doi:10.1145/3489849.3489857.
- Zhu, M., Memar, A.H., Gupta, A., Samad, M., Agarwal, P., Visell, Y., Keller, S.J., Colonnese, N., 2020. Pneusleeve: In-fabric multimodal actuation and sensing in a soft, compact, and expressive haptic sleeve, in: *Proceedings of the 2020 CHI Conference on Human Factors in Computing Systems*, Association for Computing Machinery, New York, NY, USA. p. 1–12. URL: <https://doi.org/10.1145/3313831.3376333>, doi:10.1145/3313831.3376333.
- İşleyen, A., Vardar, Y., Basdogan, C., 2020. Tactile roughness perception of virtual gratings by electrovibration. *IEEE Transactions on Haptics* 13, 562–570. doi:10.1109/TOH.2019.2959993.